

See discussions, stats, and author profiles for this publication at: <http://www.researchgate.net/publication/272405785>

Full-duplex fiber-wireless link for alternative wired and 40-GHz band wireless access based on differential quaternary phase-shift optical single sideband millimeter-wave signal

ARTICLE *in* OPTICAL ENGINEERING · FEBRUARY 2015

Impact Factor: 0.96 · DOI: 10.1117/1.OE.54.2.026101

3 AUTHORS, INCLUDING:



Jianxin Ma

Beijing University of Posts and Telecommunic...

53 PUBLICATIONS 368 CITATIONS

SEE PROFILE

Full-duplex fiber-wireless link for alternative wired and 40-GHz band wireless access based on differential quaternary phase-shift optical single sideband millimeter-wave signal

Ruijiao Zhang, Jianxin Ma,* and Xiangjun Xin

Beijing University of Posts and Telecommunications, School of Electronic Engineering, State Key Laboratory of Information Photonics and Optical Communications, Xitucheng Road #10, Haidian District, Beijing 100876, China

Abstract. A full-duplex fiber-wireless link with a uniform single sideband differential quaternary phase-shift keying optical millimeter-wave signal is proposed to provide wired or 40-GHz band wireless access alternatively. The uniform optical millimeter-wave signal that supports services for wired or wireless users is produced via an LiNbO₃ Mach-Zehnder modulator. After being transmitted to the hybrid optical network unit (HONU), it can be demodulated in different patterns on the demand of the user terminals for wired or wireless access. Simultaneously, part of the blank optical carrier abstracted from it is reused as the uplink optical carrier, so the HONU is free from the laser source, and thus, the complexity and cost of the system are reduced. Moreover, since the two tones of the dual-tone optical millimeter wave come from the same source, they maintain high coherency even after being transmitted over fiber. Additionally, the downlink data are carried by one tone of the dual-tone optical millimeter wave, so the downlink optical millimeter-wave signal suffers little from the fiber chromatic dispersion and laser phase noise. The theoretical analysis and simulation results show that our proposed full-duplex link for alternative wired and wireless access maintains good performance even when the transmission link with standard single mode fiber is extended to 30 km. © 2015 Society of Photo-Optical Instrumentation Engineers (SPIE) [DOI: [10.1117/1.OE.54.2.026101](https://doi.org/10.1117/1.OE.54.2.026101)]

Keywords: full-duplex fiber-wireless link; millimeter wave with single sideband differential quaternary phase-shift keying signal; alternative wired and wireless access.

Paper 141556 received Oct. 9, 2014; accepted for publication Jan. 5, 2015; published online Feb. 4, 2015.

1 Introduction

Nowadays, due to the ever-increasing video-based interactive and multimedia services, the current low-speed, narrow bandwidth access communications hardly meet the requirements of many bandwidth-hungry applications. The next-generation access networks aim to provide high data rates, large bandwidths, and to support flexible communications for manifold end-users in both wired and wireless accesses.¹⁻³ For wired access networks, the fiber-based optical access network can provide high-bandwidth services with large coverage, but it is still limited in applications due to the lack of mobility.⁴ On the contrary, the current wireless access networks can provide flexible and ubiquitous communication with a low deployment cost, while the data rate is still below the gigabit per second. The bandwidth requirement in wireless communications is growing drastically due to the increase of high-quality multimedia-related services with high flexibility.

Recently, radio-over-fiber (RoF) technology, bridging the gap between high-capacity (optical) and high-mobility (wireless) networks, is attracting much attention to broadband wireless access applications, including wireless backbone networks, remote medical applications, and multimedia broadcasting. So it has become a promising candidate for the future broadband wireless system⁵ because it utilizes

the optical fiber with ultrawide bandwidth and ultralow transmission loss. On the other hand, considering the architecture and network configuration, the passive optical network (PON) for the wired access with large coverage range and high capacity has good compatibility with the RoF-based wireless signal distribution networks. Therefore, in order to meet the simultaneously requirements of the huge bandwidths, high data rates, and flexible access in the next-generation access network, it is desirable to contiguously transmit broadband, baseband, and high-frequency wireless signals in an integrated platform for wired and wireless access with high spectrum efficiency. Indeed, the integrated platform, which can support the wired and wireless signals simultaneously, is a common co-shared infrastructure combining PON with RoF, as shown in Fig. 1. Such hybrid fiber-wireless access networks are foreseen to play an important role in securing a telecommunication infrastructure able to deliver wired and wireless services to the end-user in an efficient, reliable, and affordable cost per unit of bandwidth.⁶ Lately, several papers have reported on the hybrid fiber-wireless access,⁷⁻¹¹ although most of them are a simple combination of the wired and wireless transmission networks, and the wired and wireless channels are independent and only merely bonded together, which makes insufficient use of the equipment and spectrum source of the fiber. In fact, in many scenarios, either wired or wireless access is required,

*Address all correspondence to: Jianxin Ma, E-mail: majianxinxy@163.com

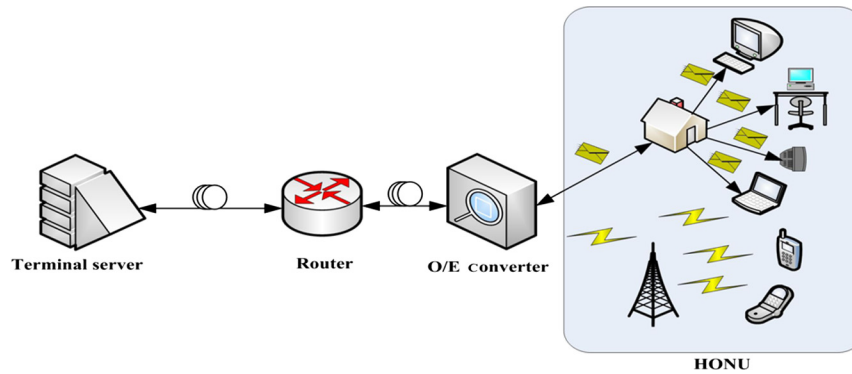


Fig. 1 The hybrid fiber-wireless access network integrated the passive optical network with radio over fiber.

so the alternative wired and wireless access with a uniform converged signal is a good choice. In such a system, each channel is designed for the uniform converged signal supporting the wired or wireless services, which improves the spectrum efficiency and reduces the structure complexity, so the system is cost-effective. In our previous study,¹² we have proposed a full-duplex hybrid fiber-wireless link with a 16-quadrature amplitude modulation (QAM) baseband signal to support the wired or wireless services alternatively using a tunable laser at the hybrid optical network unit (HONU). In this scheme, the downlink 16-QAM data are baseband modulated on the laser source, which simplifies the signal spectrum and, thus, improves the spectrum efficiency, but a tunable laser is needed at the HONU to provide the coherent optical local oscillator, which makes the HONU complex and expensive.

In this paper, we have proposed a full-duplex link with a uniform optical millimeter-wave signal to provide the alternative wired and wireless access. In the central station (CS), the uniform optical millimeter-wave signal is generated by an LiNbO₃ Mach-Zehnder modulator (LN-MZM) in single sideband (SSB) pattern. Although the SSB optical millimeter-wave signal is usually used in the RoF link for wireless access, the uniform optical millimeter-wave signal has a large optical carrier-to-sideband ratio (CSR) and can be demodulated in different patterns to support wired or wireless access alternatively. The SSB modulation adopted in our scheme improves the spectrum efficiency and makes the downlink signal suffer little from the fiber chromatic dispersion. At the HONU, the downlink optical signal is switched into different receiver modules for wired or wireless access based on the heterodyne detection or the optical differential quaternary phase-shift keying (DQPSK) receiver.¹³ For the uplink, part of the optical carrier is reused to carry the uplink signals and modulated by the 40-GHz DQPSK millimeter wave or the baseband DQPSK uplink signal. The demodulation module for the wired or wireless uplink signals is the same as the downlink wired access, which makes sufficient use of the equipment of the CS and, thus, simplifies the CS. Moreover, since the uplink optical carrier is abstracted from the downlink, the HONU needs no laser source and, so, is cost-effective. To verify the feasibility, a full-duplex link for alternative wired or wireless access is built up based on the simulation platform. According to the evaluation of the simulated signals of both downlink and uplink for either wired or wireless access,

it can be seen that the proposed full-duplex link has good performance in providing both wired and wireless access.

The rest of the paper is arranged as follows. In Sec. 2, the principle of the proposed full-duplex link for the alternative wired and wireless access is described and theoretically analyzed in detail. In Sec. 3, a proof-of-concept of a full-duplex fiber-wireless access link with 10-Gbit/s DQPSK downlink and uplink for the bidirectional wired optical access and RoF-based 40-GHz band wireless access is built up based on the simulation platform and the simulation results are analyzed in detail. At last, a conclusion is drawn in Sec. 4.

2 Principle of Operation

Figure 2 shows the scheme diagram of our proposed full-duplex fiber-wireless access network capable of providing gigabit wired and wireless access alternatively based on wavelength division multiplexing PON, which consists of the CS, HONU, wired, and wireless user terminals. In the CS, the transmitted downlink data with DQPSK format, which consists of *I*- and *Q*-branches, can be expressed as

$$\begin{bmatrix} I(t) \\ Q(t) \end{bmatrix} = \begin{bmatrix} \sum_n a_{I,n} g_T(t - nT_s) \\ \sum_n a_{Q,n} g_T(t - nT_s) \end{bmatrix}. \quad (1)$$

Here, $a_{I,n}$ and $a_{Q,n}$ are the binary differential digital signal serials, $a_{I/Q,n} = \{-1, 1\}$; $g_T(t)$ is the code shape function and T_s is the symbol interval. The *I*- and *Q*-branches of the baseband DQPSK signal are mixed with the radio frequency (RF) sinusoidal clock $V_m(t) = V_m \cos \omega_m t$ and $V_m(t) = -V_m \sin \omega_m t$, respectively, and the generated RF-DQPSK signal can be expressed as

$$\begin{aligned} D_{\text{RF-DQPSK}}(t) &= V_m [I(t) \cos \omega_m t - Q(t) \sin \omega_m t] \\ &= V_m \sqrt{I(t)^2 + Q(t)^2} \cos[\omega_m t + \varphi_i(t)] \\ &= \sqrt{2} V_m \cos[\omega_m t + \varphi_i(t)]. \end{aligned} \quad (2)$$

Here, V_m and ω_m are the amplitude and angular frequency of the RF clock, respectively, and $\varphi_i(t) = \arctan Q(t)/I(t) = \pi/4, 3\pi/4, 5\pi/4,$ and $7\pi/4$ for $i = 1, 2, 3,$ and 4 , respectively.

The light wave emitted from the continuous wave laser with a central frequency of $f_0 = \omega_0/2\pi$, expressed as $E(t) = E_0 \exp(j\omega_0 t)$, is modulated by the RF-DQPSK

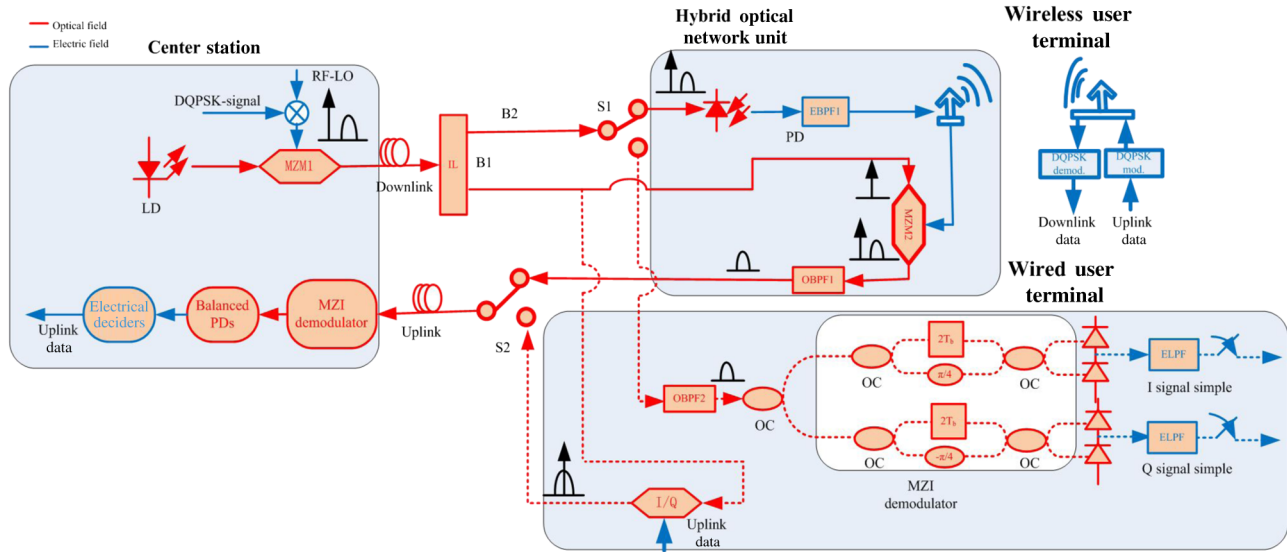


Fig. 2 The full-duplex fiber-wireless link for alternative wired and wireless access. LD, laser diode; MZM, Mach-Zehnder modulator; OBPF, optical band-pass filter; PD, photodiode; EBPF, electrical band-pass filter; ELPF, electrical low-pass filter; MZI, Mach-Zehnder interferometer; I/Q, I/Q modulator.

signal in an SSB pattern via an LiNbO₃ Mach-Zehnder modulator (LN-MZM1), as shown in Fig. 2. Since the negative first-order sideband is suppressed and the higher-order sidebands can be ignored due to their negligible power, the generated uniform SSB-DQPSK optical millimeter-wave signal with two main tones, the blank optical carrier at ω_0 and the positive first-order sideband at $\omega_0 + \omega_m$, can be expressed as

$$\begin{aligned}
 E_{\text{SSB}}(0, t) &\approx \frac{E_0 \gamma_1}{2} \left[\sqrt{2} J_0(m_{h1}) e^{j\omega_0 t} + 2 J_1(m_{h1}) e^{j[(\omega_0 + \omega_m)t - \phi_i(t)]} \right] \\
 &= E_C e^{j\omega_0 t} + E_S e^{j[(\omega_0 + \omega_m)t - \phi_i(t)]}.
 \end{aligned} \quad (3)$$

Here, the modulation index is defined as $m_{h1} = \pi \sqrt{2} V_m / V_\pi$; γ_1 is the additional insertion loss of LN-MZM1. Usually, the modulation index is smaller, therefore, $J_0(x) \approx 1$ and $J_1(x) \approx x$, so $E_C = \sqrt{2} E_0 \gamma_1 / 2$ and $E_S = m_{h1} E_0 \gamma_1$, in Eq. (3), represent the amplitudes of the blank optical carrier and the first-order sideband, respectively. From Eq. (3), we can see that the optical carrier at ω_0 has a constant amplitude and phase, while the first-order sideband carries the phase information of the DQPSK data with a constant amplitude. Since the optical carrier is larger than the first-order sideband, the generated SSB optical millimeter-wave signal has a large optical CSR. It is worth noting that the SSB modulation is adopted here, which improves the spectrum efficiency. The two tones of the SSB optical millimeter-wave signal come from the same laser source, which assures they have good coherency. If the nonlinearity is neglected, the fiber transmission function with the length of z can be expressed in the frequency domain as

$$H(\omega) = e^{-[\alpha + j\beta(\omega)]z}. \quad (4)$$

After being transmitted over the chromatic fiber with the amplitude attenuation coefficient of α and propagation

constant of $\beta(\omega)$ at the angular frequency of ω , the uniform SSB-DQPSK optical millimeter-wave signal can be developed mathematically as

$$\begin{aligned}
 E_{\text{SSB}}(z, t) &= F^{-1}\{H(\omega)F[E_{\text{SSB}}(0, t)]\} \\
 &\approx E_C e^{-\alpha z} e^{j[\omega_0 t - \beta(\omega_0)z]} \\
 &\quad + E_S e^{-\alpha z} e^{j\{(\omega_0 + \omega_m)t - \beta(\omega_0 + \omega_m)z - \phi[t - (\omega_0 + \omega_m)^{-1}\beta(\omega_0 + \omega_m)z]\}} \\
 &= E_C(z, t) + E_S(z, t).
 \end{aligned} \quad (5)$$

Here, $F\{\}$ and $F^{-1}\{\}$ are the forward and inverse Fourier transforms, respectively. From Eq. (5), we see that, after the fiber transmission, the amplitudes of two tones are attenuated exponentially due to the fiber loss. And although a phase shift is induced between the two tones because of the fiber chromatic dispersion, the downlink DQPSK signal, which is carried by the sideband, suffers no degradation.

At the HONU, an interleaver (IL) with finite isolation is employed to divide the uniform downlink SSB-DQPSK optical millimeter-wave signal into two beams. One is the blank optical carrier at ω_0 , while the other consists of the suppressed optical carrier and the optical sideband at $\omega_0 + \omega_m$. The latter can be switched into the designated optoelectrical conversion modules by an optical switch (S1) for either wired or wireless access according to the requirement of the user terminals. The dotted and solid lines in Fig. 2 show the wired and wireless accesses, respectively.

For the wireless access, the SSB optical millimeter-wave signal with the suppressed optical carrier is directed to a high-speed square-law photo-diode (PD) to generate an electrical millimeter wave at ω_m based on self-heterodyne beating. Since the optical carrier is properly suppressed, the CSR is reduced close to the optimized value, so the SSB optical millimeter-wave signal has a higher detection sensitivity. Equation (6) shows the photocurrent of the electrical millimeter-wave signal

$$I_{\text{down-wireless}}(t) = \mu' E_0^2 \gamma_1^2 e^{-2\alpha z} \left(\frac{1}{2} + m_{h1}^2 \right) + \sqrt{2} m_{h1} \mu' E_0^2 \gamma_1^2 e^{-2\alpha z} \cos(\omega_m t + \varphi_i - \Delta\varphi). \quad (6)$$

Here, μ' is the sensitivity of the PD for the wireless access at the HONU, and $\Delta\varphi = \beta(\omega_0 - \omega_m)z - \beta(\omega_0)z$ denotes the phase shift between the optical carrier and the first-order sideband. It should be pointed out that the phase-modulation signal is retained in the RF signal at ω_m , which will be abstracted out by an electrical filter with the central frequency of ω_m and radiated to the wireless users through the antenna after amplification. At the user terminals, the RF signal received by antenna is first divided into two beams by an electrical power splitter. Then the upper and lower beams are separately mixed with $V_{\text{LO1}}(t) = V_{\text{LO1}} \cos \omega_{\text{LO}} t$ and $V_{\text{LO2}}(t) = V_{\text{LO2}} \sin \omega_{\text{LO}} t$ to realize the electrical coherent demodulation. After two electrical low-pass filters, we can obtain the I - and Q -branches of the baseband signal. Here, ω_{LO} is equal to the frequency of the RF signal. Since the downlink data are carried by only one tone of the dual-tone optical millimeter-wave, the fiber chromatic dispersion has little effect on the heterodyne RF signal.

For the wired access, the data-bearing optical sideband at $\omega_0 + \omega_m$ is separated away from the suppressed optical

$$E_{\text{DR-MZI-I}}(z, t) = \begin{bmatrix} E_{\text{output 1}}(z, t) \\ E_{\text{output 2}}(z, t) \end{bmatrix} = \frac{1}{2} \begin{bmatrix} -j(E_S(z, t - T_s) + E_S(z, t)e^{j\pi/4}) \\ -E_S(z, t - T_s) + E_S(z, t)e^{j\pi/4} \end{bmatrix} \quad (9)$$

$$E_{\text{DR-MZI-Q}}(z, t) = \begin{bmatrix} E_{\text{output 3}}(z, t) \\ E_{\text{output 4}}(z, t) \end{bmatrix} = \frac{1}{2} \begin{bmatrix} -j(E_S(z, t - T_s) + E_S(z, t)e^{-j\pi/4}) \\ -E_S(z, t - T_s) + E_S(z, t)e^{-j\pi/4} \end{bmatrix}.$$

Then, two balanced detectors following the MZIs are used to convert the optical signals to the electrical ones. Each balanced detector pair consists of two square-law PDs, as shown by the inset in Fig. 2. Considering the balanced configuration of the receiver, the output photocurrents of the received signal can be expressed as

$$I_{\text{down-wired}}(z, t) = I_1(z, t) - I_2(z, t) = \mu [|E_{\text{output 1}}(z, t)|^2 - |E_{\text{output 2}}(z, t)|^2] = \mu E_0^2 \gamma_1^2 m_{h1}^2 e^{-2\alpha z} \cos \left[\varphi(t - T_s) - \varphi(t) + \frac{\pi}{4} + T_s(\omega_0 - \omega_m) \right],$$

$$I_{\text{down-wired}}(z, t) = I_3(z, t) - I_4(z, t) = \mu [|E_{\text{output 3}}(z, t)|^2 - |E_{\text{output 4}}(z, t)|^2] = \mu E_0^2 \gamma_1^2 m_{h1}^2 e^{-2\alpha z} \cos \left[\varphi(t - T_s) - \varphi(t) - \frac{\pi}{4} + T_s(\omega_0 - \omega_m) \right]. \quad (10)$$

Here, $\varphi(t - T_s)$ represents the phase information of the next symbol. It can be seen from Eq. (10) that the DQPSK optical signal is converted to the electrical baseband QPSK signal with two tributaries. Then the electrical photocurrents pass through a decider, respectively, to recover the I - and Q -branches of the downlink data.

carrier by an optical band-pass filter with the central frequency of $\omega_0 + \omega_m$ or a second IL. Then it is demodulated by the DQPSK demodulator based on a Mach-Zehnder interferometer (MZI), as shown in Fig. 2. The DQPSK demodulator consists of two sets of MZIs, namely the I -MZI and Q -MZI, to detect the in-phase (I) and quadrature (Q) tributaries, respectively. In each MZI, the time delay between the two branches is equal to one symbol interval T_s ; then, two pairs of balanced receivers, low-pass filters, and samplers follow.¹³ There exists an additional phase shift of $\pi/4$ and $-\pi/4$ at the lower branch in I -MZI and Q -MZI, respectively, as shown by the inset in Fig. 2. Since the MZI can be regarded as the cascade of the Y branch, parallel transmission lines and Y branch, their transfer functions can be expressed in the frequency domain as

$$H_I(f) = \frac{1}{2} \begin{bmatrix} e^{-j2\pi f T_s} - e^{j\pi/4} & -j(e^{-j2\pi f T_s} + e^{j\pi/4}) \\ -j(e^{-j2\pi f T_s} + e^{j\pi/4}) & e^{j\pi/4} - e^{-j2\pi f T_s} \end{bmatrix}, \quad (7)$$

$$H_Q(f) = \frac{1}{2} \begin{bmatrix} e^{-j2\pi f T_s} - e^{-j\pi/4} & -j(e^{-j2\pi f T_s} + e^{-j\pi/4}) \\ -j(e^{-j2\pi f T_s} + e^{-j\pi/4}) & e^{-j\pi/4} - e^{-j2\pi f T_s} \end{bmatrix}. \quad (8)$$

After the MZIs, two pairs of optical beams are generated and can be expressed in the time domain as

For the uplink, at the HONU, the optical carrier at ω_0 abstracted from the downlink is reused to carry the uplink signals. The uplink baseband DQPSK data $S_{\text{up}}(t) = I_{\text{up}}(t) + jQ_{\text{up}}(t)$ for wired access or the uplink RF-DQPSK signal at ω_{up} from the antenna for wireless access is modulated on it via an optical I/Q modulator or an LN-MZM2, respectively. The data-bearing uplink optical signal for wired access is obtained as

$$E_{\text{up-wired}}(0, t) = \gamma_2 E_C' e^{j\omega_0 t} \left[\sin \pi \frac{V_{\text{up}}}{V_\pi} I_{\text{up}}(t) + \sin \pi \frac{V_{\text{up}}}{V_\pi} Q_{\text{up}}(t) \right] \approx \gamma_2 m_{h2} E_C' e^{j\omega_0 t} [I_{\text{up}}(t) + jQ_{\text{up}}(t)]. \quad (11)$$

Here, $E_C' = e^{-(\alpha + j\beta(\omega_0))z}$, $m_{h2} = \pi V_{\text{up}}/V_\pi$ is the uplink modulation index, γ_2 is the insertion loss of the I/Q modulator, and the approximation is proper if m_{h2} is smaller. The uplink optical signal of the wireless access is SSB modulated on the optical carrier. After that, the generated SSB uplink optical millimeter-wave signal is converted to the baseband by only abstracting the optical sideband at $\omega_0 + \omega_{\text{up}}$ bearing the uplink data, which simplifies the optical spectrum and, thus, improves the spectrum efficiency. Here, we note that since the optical carriers for uplinks are abstracted from the downlink signal, the HONU is free from the laser source, so its structure is simplified and the cost is reduced.

After being transmitted back to the CS through the uplink with the z' -length fiber, the uplink optical signal for wired access becomes

$$E_{\text{up-wired}}(z', t) = \gamma_2 m_{h2} E'_C [I_{\text{up}}(t - \tau') + jQ_{\text{up}}(t - \tau')] e^{-\alpha z} e^{j[\omega_0 t - \beta(\omega_0)z']}. \quad (12)$$

Here, the uplink transmission delay is $\beta'(\omega_0)z' = \tau'$ for the wired access. In the CS, similar to the demodulation module of the downlink DQPSK optical signal for wired access, two MZIs with two pairs of balanced detectors are coshared to demodulate the uplink baseband optical signal for either wired or wireless access. It is worth noting that, for the uplink, the receiver module for wireless access is coshared with the wired access, which simplifies the CS. Therefore, the proposed scheme realizes the full-duplex alternative wired and wireless access.

The proposed scheme can realize the full-duplex wired or RoF access alternatively according to the requirement of the user terminals since the uniform optical millimeter-wave signal can be decomposed as the optical baseband or optical millimeter-wave signal at the HONU. According to the theoretical analysis above, our proposed scheme has many advantages. First, since the proposed full-duplex channel with a uniform optical millimeter-wave signal can provide the wired or wireless access alternatively, it realizes a deeper integration of wired and wireless access in the signal. Second, the influence of the fiber chromatic dispersion is reduced and the spectrum efficiency is improved since the SSB modulation is adopted. Third, in the uplink, reusing the blank optical carrier to carry the uplink signal makes the HONU free from the laser source and, thus, makes the HONU simple and cost-effective. At last, for the wired access, the full-duplex link has a symmetrical received structure, and for the uplink, the receiver module for wireless

access is coshared with the wired access, which simplifies the CS.

3 Simulation Setup and Results

To verify our proposed full-duplex link for the alternative wired and wireless access scheme, a proof-of-concept link is set up based on the OptiSystem simulation platform. The full-duplex optical link can be switched into the wired access, as shown in Fig. 3, or into the wireless access as shown in Fig. 5, alternatively. In the CS, to generate the uniform optical millimeter-wave signal, a continuous light wave with the frequency of 193.1 THz and line width of 100 kHz emitted from a laser source is injected into a dual-drive LN-MZM with the half-wave voltage of 4 V and modulated by the RF-DQPSK signal in the SSB pattern. The RF-DQPSK signal is generated by a 40-GHz RF clock mixing with the baseband DQPSK signal mapped from a 10-Gbit/s pseudorandom binary sequence with a word length of $2^{11} - 1$. After being filtered by an optical band-pass filter with the central frequency at 193.12 THz and bandwidth of 70 GHz, the downlink uniform SSB-DQPSK optical millimeter-wave signal mainly consists of two optical tones with a CSR of 20 dB, as shown by Fig. 3(a). The sideband at 193.14 THz carries the downlink DQPSK data, while the other at 193.1 THz is the blank optical carrier. For the wireless access, the latter works as the referenced optical local oscillator to convert the baseband optical signal to the millimeter-wave one. It is also reused as the uplink optical carrier for either wired or wireless access at the HONU. Then, the two optical tones with a frequency spacing of 40 GHz are transmitted forward to the HONU over the standard single-mode fiber with the chromatic dispersion of 16.75 ps/nm · km, power attenuation of 0.2 dB/km, and dispersion slope of 0.075 ps/nm² · km.

At the HONU, an IL with the frequency spacing of 40 GHz and depth of 20 dB is used to abstract the optical carrier at 193.1 THz from the received uniform downlink

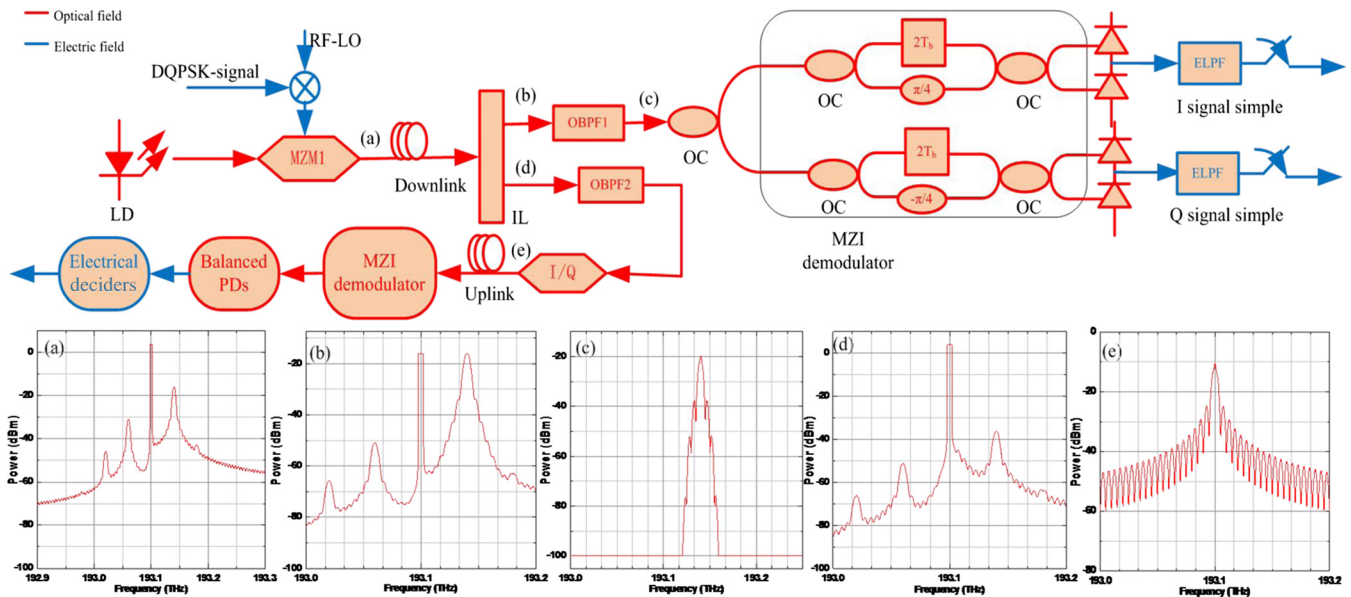


Fig. 3 Simulation setup of the proposed full-duplex fiber-wireless link for wired access and the optical spectra of the signals with the resolution of 0.1 nm at (a) the output of the LN-MZM1, (b) the upper output of the IL, (c) the output of the optical band-pass filter, (d) the lower output of the IL, and (e) the output of the I/Q modulator.

optical millimeter-wave signal for carrying the uplink signal, as shown by the spectrum in Fig. 3(d). We can see that the CSR of the SSB optical millimeter-wave signal output from the IL is reduced from 20 to 0 dB since the optical carrier is suppressed, as shown by the spectrum in Fig. 3(b). Then the abstracted optical carrier is modulated in different patterns for either wired PON access or RoF-based wireless access. The full-duplex optical link works as a PON for the wired access by switching to the wired port, as shown in Fig. 3. The data-bearing optical sideband at 193.14 THz is separated from the blank optical carrier by an optical band-pass filter with the central frequency of 193.14 THz and a bandwidth of 20 GHz, as shown by the spectrum in Fig. 3(c). And it is input into the MZI demodulator following two pairs of balanced PDs to recover the electrical baseband with *I*- and *Q*-branches. The responsivity and the dark current of the PDs are 1 mA/mW and 10 nA, respectively. For the uplink of the wired access, the blank optical carrier from the IL at 193.1 THz is modulated by the uplink baseband DQPSK signal via a nested I/Q modulator with the half-wave voltage of 4 V. After the optical I/Q modulation, the data-bearing baseband uplink optical signal, as shown by the spectrum in Fig. 3(e), is transmitted to the CS over the uplink. In the CS, the receiver module, which is the same as the downlink receiver, is used to demodulate the uplink baseband optical signal to the electrical one with *I*- and *Q*-branches.

To check the wired access performance of the uniform optical millimeter-wave signal, introducing a white light source with a power of -29 dBm (the resolution is 0.1 nm) at the receiver terminal, the error vector magnitude (EVM) curves and the corresponding constellations at a

certain received optical power of the downlink and uplink QPSK signals are measured, as illustrated in Fig. 4. The measured bit error rate (BER) curves versus optical signal to noise ratio (OSNR) at different transmissions are shown in Fig. 5. According to Ref. 14, the EVM is essentially the normalized error magnitude between the measured constellation and the ideal constellation, which can be obtained from the optimized constellation diagrams and can be expressed as

$$EVM = \frac{\sqrt{\frac{1}{N} |S_r(n) - S_t(n)|^2}}{R_{max}}, \tag{13}$$

where *N* is the number of transmitted symbols, *S_r* is the normalized received symbol, *S_t* is the ideal transmitted symbol, and *R_{max}* is the maximum magnitude of the ideal transmitted symbol for the chosen modulation. In our paper, based on the definition of the EVM, we calculate the EVM according to the simulation data of the constellation diagrams.

Considering M-ary constellation, the relationship between the EVM and BER for the 4-QAM vector signal can be expressed by¹⁴

$$BER = Q\left(\frac{1}{EVM}\right), \tag{14}$$

where *Q*(·) is the Gaussian co-error function and is given by

$$Q(x) = \int_x^\infty \frac{1}{\sqrt{2\pi}} e^{-\frac{y^2}{2}} dy. \tag{15}$$

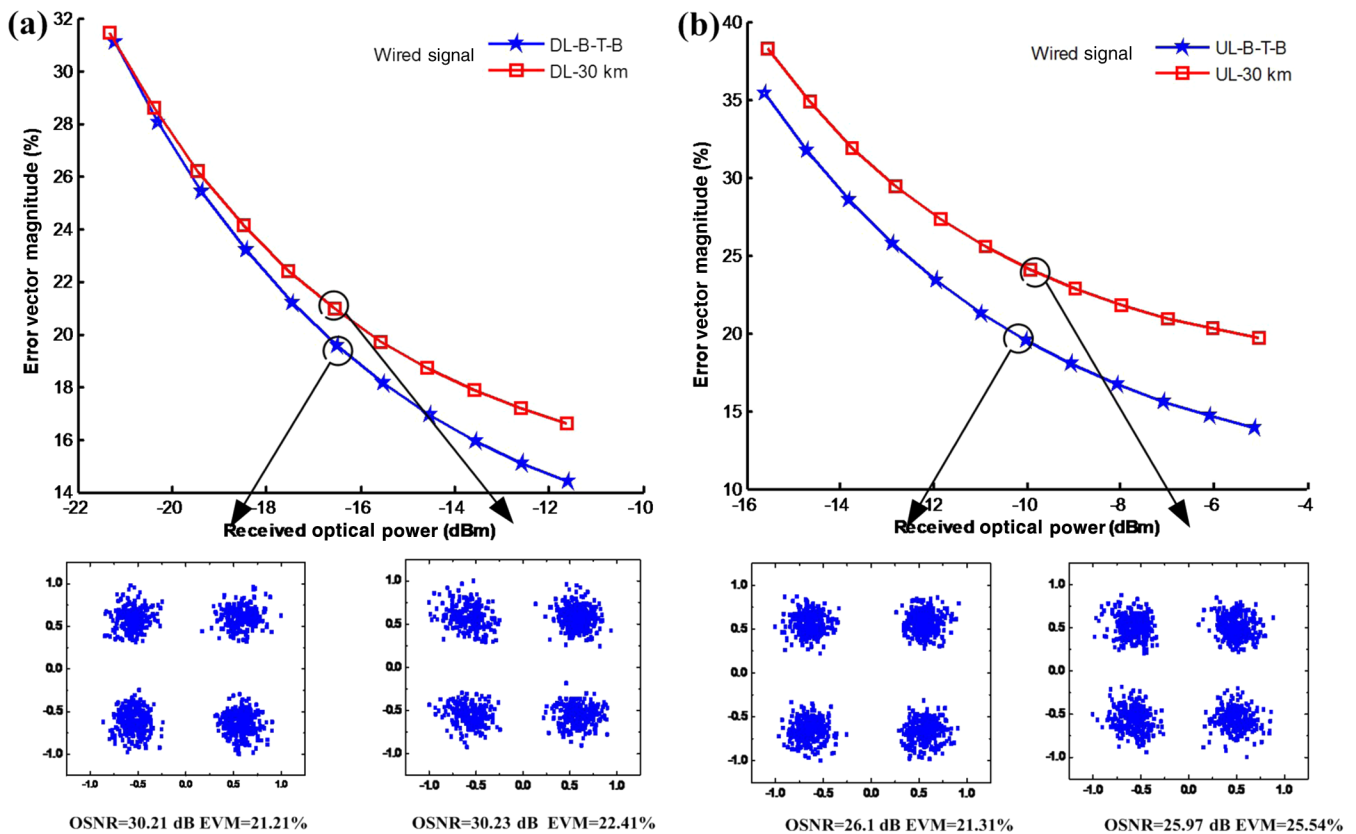


Fig. 4 EVM versus received optical power for the wired signals: (a) downlink and (b) uplink.

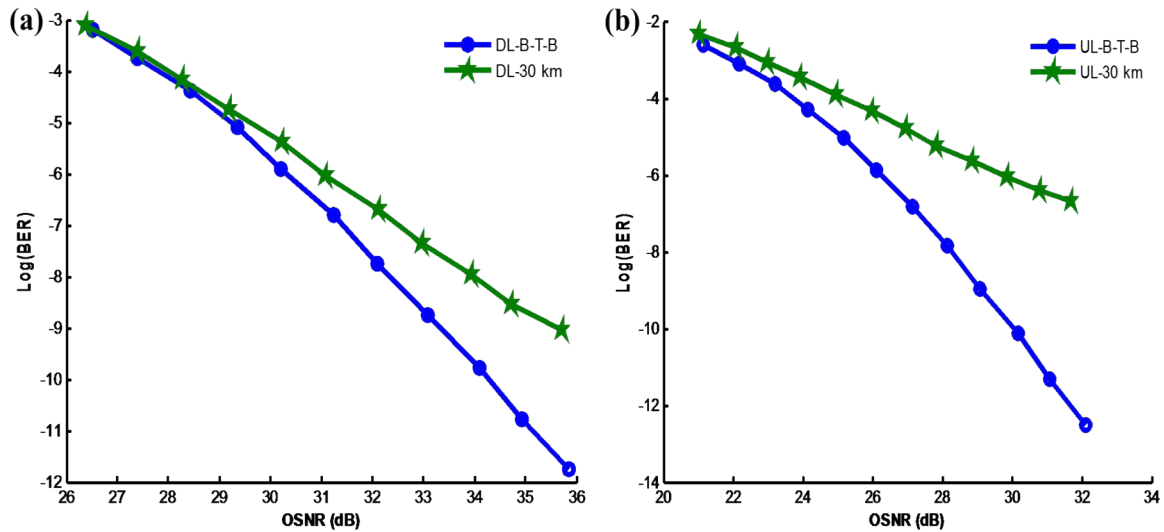


Fig. 5 Measured BER performance versus OSNR in back-to-back (B-T-B) case and after 30 km transmission for wired signals: (a) downlink and (b) uplink.

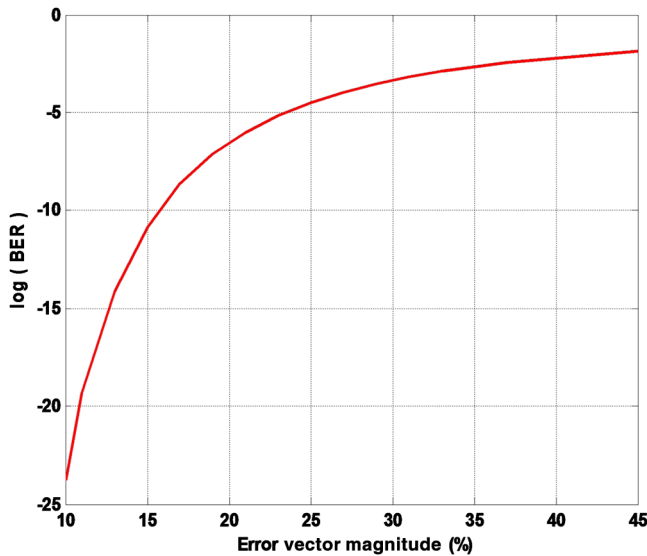


Fig. 6 The conversion relationship between EVM and BER for a 4-QAM vector signal.

Figure 6 shows the curve of BER versus EVM for a 4-QAM vector signal. The conversion relationship between EVM and BER for QPSK vector signal is the same as that for 4-QAM.

The results in Fig. 4 show that with the reduction of the received optical power, the EVMs of the downlink and uplink increase. The required received optical power at a BER of $\sim 1 \times 10^{-6}$ for the downlink in the back-to-back (B-T-B) case is ~ -17.5 dBm. Less than 1-dB power penalty after 30 km fiber transmission is observed compared to B-T-B case. But when the received optical power is < -20 dBm, the transmission performance of the link after 30 km fiber transmission is the same as that of the link in the B-T-B case, which may be because the fiber loss is no longer the main factor impacting the transmission performance. For the uplink, the power penalty is ~ 1 dB. Comparing Fig. 4(a) with Fig. 4(b), we can find that

when the EVM of the downlink is equal to the uplink, the required received optical power of the downlink is smaller than the uplink. These results can be attributed to the fact that the blank optical carrier is abstracted from the downlink with a smaller power and, thus, has a small OSNR. The clear constellations of the downlink and uplink QPSK signals at -17.45 and -10.98 dBm received optical power in the B-T-B case and after 30 km transmission at -17.52 and -10.9 dBm are shown in the insets of Fig. 4. According to the relationship between EVM and BER for the QPSK vector signal,¹⁴ the BERs for the above conditions are 1.22×10^{-6} , 1.35×10^{-6} , 4.05×10^{-6} , and 4.52×10^{-6} , respectively. We can see that even though the constellation points have a smaller dispersion after 30 km fiber transmission, they do not overlap with each other and can be distinguished clearly. And from Fig. 5, we can see that the required OSNR at BER of $\sim 1 \times 10^{-6}$ in B-T-B case is ~ 30.5 dB. After 30 km transmission, the corresponding OSNR penalty is ~ 1 dB. For the uplink, the OSNR penalty is ~ 3 dB at a BER of 1×10^{-6} . All these assure the feasibility of the proposed full-duplex link for the wired access.

For the RoF-based wireless access, the full-duplex link is configured by switching to the wireless port, as shown in Fig. 7. Since the downlink before the optical switch changes little, the simulation results of the optical signals are identical with the wired case so we do not repeat them here. At the HONU, the SSB optical millimeter-wave signal with the CSR of 0 dB, as shown in Fig. 3(b), is directed to the high-speed PD with the bandwidth of 40 GHz for self-heterodyne beating to generate the 40-GHz millimeter wave. The responsivity and the dark current of the PD are 1 mA/mW and 10 nA, respectively. Then the 40-GHz electrical millimeter wave is filtered out by an electrical band-pass filter with a central frequency at 40 GHz and a bandwidth of 15 GHz, as shown by the RF spectrum in Fig. 7(a).

For the uplink, similar to the wired access, the abstracted blank optical carrier that is used as the uplink optical carrier is modulated by the 10-Gbit/s 40-GHz RF-DQPSK signal received by the antenna via LN-MZM2 with the half-wave voltage of 4 V such as that of the downlink signal, and the output SSB optical millimeter-wave signal has the

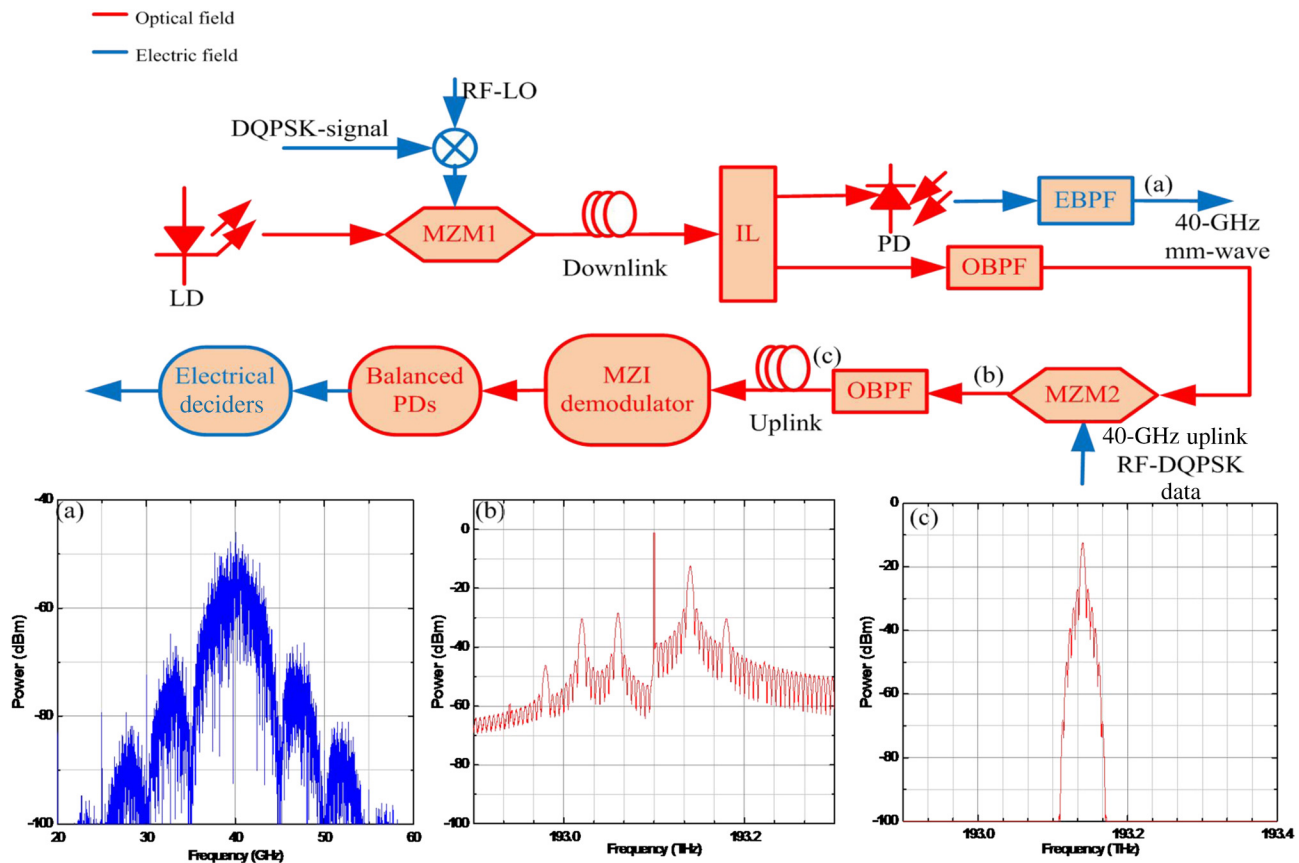


Fig. 7 Simulation setup of the proposed full-duplex fiber-wireless link for wireless access and the electrical spectrum of the signal at (a) the output of the electrical band-pass filter, and the optical spectra of the signals at (b) the output of the LN-MZM2, and (c) the output of the optical band-pass filter.

spectrum as given in Fig. 7(b). The broadened optical sideband at 193.14 THz carrying the uplink data is filtered out by an optical filter with a central frequency of 193.14 THz and a bandwidth of 30 GHz, as shown by the spectrum in Fig. 7(c). By this means, the optical millimeter-wave signal is down-converted to the baseband in the optical domain, which occupies a much narrower bandwidth. Then the filtered optical sideband is transmitted back to the CS over the fiber uplink. In the CS, the uplink baseband optical signal can be demodulated by the same receiver module for the wired access uplink.

In order to check the performance of the downlink for wireless access, the generated 40-GHz DQPSK millimeter-wave signal is directly coherently demodulated back to the baseband by a 40-GHz electrical local oscillator without wireless propagation here, because what we are interested in are the transmission performance of the unified common optical signal in optical domain and how the electrical signal is converted from unified common optical signal for the wired and wireless access, rather than to study the wireless transmission performance of the RF signal. Even though in the real system, the wireless transmission performance of the millimeter-wave signal is also important, it is out of the scope of our paper. Figures 8 and 9 present the measured EVM curves with the corresponding constellation diagrams of the downlink and uplink DQPSK signals, and the BER curves for wireless access, respectively. It can be seen that in Fig. 8, as the wired access, the EVMs increase

with the reduction of the received optical power, and when the EVMs of the downlink and uplink are equal, the received optical power of the downlink is also smaller than the uplink. But comparing Fig. 4 with Fig. 8, we can see that when the received optical power of the downlink in the B-T-B case is ~ -20 dBm for the wired access, the EVM is $\sim 28.03\%$ ($\text{BER} = 1.8 \times 10^{-4}$), while for the wireless access, the EVM is $\sim 35.5\%$ ($\text{BER} = 2.8 \times 10^{-3}$), which exceeds the forward error correction limit.¹⁵ This indicates the required received optical power range of the wired access is larger than that of the wireless access. The reason is that for the wired access, a coherent receiver is used, which can improve the receiving sensitivity compared with the direct detection. From Fig. 8, it can also be seen that when the received optical power is > -19 dBm for the downlink and -14 dBm for the uplink after 30 km fiber transmission, the EVM is still $< 35.2\%$ ($\text{BER} = 2.3 \times 10^{-3}$), so the full-duplex link for wireless access can realize error-free transmission. The corresponding constellation diagrams in the insets of Fig. 8 show that after 30 km fiber transmission, the constellation points of the downlink and uplink signals have a small dispersion as with the wired access due to the chromatic dispersion and nonlinear effects of the optical link, but they still maintain good convergence, which indicates that the good performance of the downlink and uplink signals is assured. As expected in Sec. 2, this is attributed to the fact that the SSB modulation in our scheme can reduce the influence of the fiber dispersion on the heterodyne RF

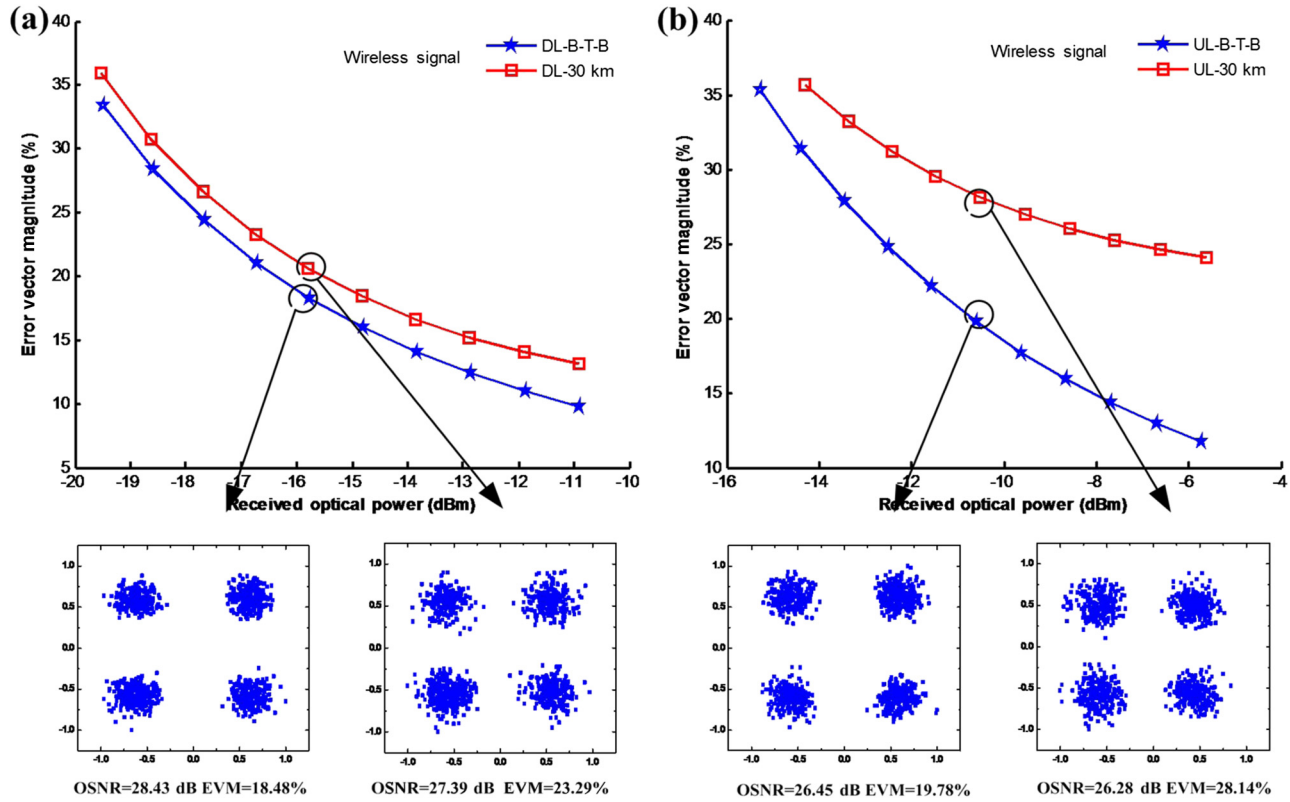


Fig. 8 EVM versus received optical power for wireless signals: (a) downlink and (b) uplink.

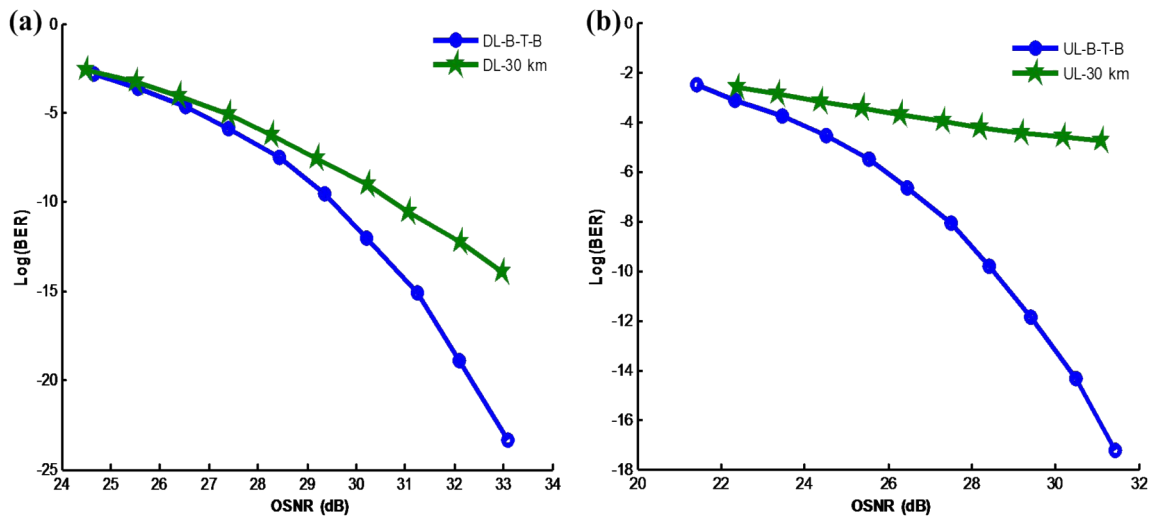


Fig. 9 Measured BER performance versus OSNR in B-T-B case and after 30 km transmission for wireless signals: (a) downlink and (b) uplink.

signal. For the wireless access uplink, the effect of the fiber chromatic dispersion is greatly reduced by downconverting the optical millimeter-wave signal to the baseband one with a much narrower bandwidth in the optical domain. Figure 9 shows that the OSNR penalty for a wireless downlink is ~ 1.5 dB after 30 km transmission at the BER of 1×10^{-6} , while for the uplink, after 30 km transmission, the BER curve has the lowest floor, which is $\sim 1 \times 10^{-5}$, and does not decrease with the increase of the OSNR. The OSNR penalty at the BER of 1×10^{-4} is ~ 5 dB. The simulation results

agree with the theoretical analysis and show that our proposed full-duplex link can provide a good insight into the performance for the wireless access even when the transmission link is extended to 30 km.

4 Conclusion

A full-duplex fiber-wireless network architecture with a uniform 10-Gbit/s DQPSK optical millimeter-wave signal based on SSB modulation supporting alternative wired and 40-GHz band wireless accesses is proposed. At the

HONU, the downlink uniform SSB-ODQPSK millimeter-wave signal is switched into different receiver modules for wired or wireless access according to the requirement of the end users. In our scheme, since the downlink data are modulated in an SSB pattern, the downlink signal suffers little from fiber chromatic dispersion and laser phase noise because of the good coherency between the two tones coming from the same source, so the transmission distance is extended. Since the uplink optical carrier is abstracted from the downlink signal, the optical source of the uplink at the HONU is unnecessary for either wired or wireless access. This makes the HONU free from the laser source and more cost-effective. Moreover, whether the wired or wireless access pattern is chosen at the HONU and the downlink optical signal has a uniform format, which simplifies the structure of the signal spectrum, the complexity of the CS, and the fiber access network. Additionally, the receiver module for the wired or wireless uplink signal is the same in the CS, which further simplifies the structure of the CS. The proposed scheme realizes the total integration of the wired and wireless access by using the wired-wireless uniform optical signal. Both the theoretical analysis and the simulation results demonstrate the feasibility of our proposed full-duplex access link for delivering broadband services. It is expected that the proposed wired and wireless integrated network will be implemented in future fiber-wireless network architectures for providing alternative wired and wireless access.

Acknowledgments

This work was supported in part by the Program for New Century Excellent Talents in University with Grant No. NECT-11-0595 and the National Natural Science Foundation of China (NSFC, Grant 61425022).

References

1. J.-C. Lin et al., "Hybrid optical access network integrating fiber-to-the-home and radio-over-fiber systems," *IEEE Photon. Technol. Lett.* **19**(8), 610–612 (2007).
2. A. Martinez, V. Polo, and J. Marti, "Simultaneous baseband and RF optical modulation scheme for feeding wireless and wireline heterogeneous access network," *IEEE Trans. Microw. Theory Tech.* **49**(10), 2018–2024 (2001).
3. C. Lim et al., "Millimeter-wave broad-band fiber-wireless system incorporating baseband data transmission over fiber and remote LO delivery," *J. Lightwave Technol.* **18**(10), 1355–1363 (2000).
4. Y. Guo, L. C. Ong, and M.-T. Zhou, "Microwave photonic 60-GHz wireless link for gigabit connectivity," in *IEEE 19th Int. Symp. on Personal, Indoor and Mobile Radio Communications*, pp. 1–5, IEEE (2008).
5. Z. Jia et al., "Key enabling technologies for optical-wireless networks: optical millimeter-wave generation, wavelength reuse, and architecture," *J. Lightwave Technol.* **25**(11), 3452–3471 (2007).
6. I.-T. Monroy et al., "Converged wireline and wireless signal transport over optical fiber access links," in *14th Opto-Electronics Communication Conf.*, pp. 1–2, IEEE (2009).
7. C.-Y. Li et al., "Generation and transmission of BB-MW-MMWs by cascading PM and MZM," *J. Lightwave Technol.* **30**(3), 298–303 (2012).
8. C.-W. Chow and Y.-H. Lin, "Convergent optical wired and wireless long reach access network using high spectral efficient modulation," *J. Opt. Express* **20**(8), 9243–9248 (2012).
9. Z. Cao et al., "WDM-RoF-PON architecture for flexible wireless and wire-line layout," *J. Opt. Commun. Neww.* **2**(2), 117–121 (2010).
10. M. F. Huang et al., "Integration of RoF with WDM-PON for lightwave centralized access network," in *16th Opto-Electronics and Communication Conf.*, pp. 387–388, IEEE (2011).
11. L. Zhang et al., "Simultaneous generation of independent wired and 60-GHz wireless signals in an integrated WDM-PON-RoF system based on frequency-sextupling and OCS-DPSK modulation," *J. Opt. Express* **20**(13), 14648–14655 (2012).
12. R. Zhang et al., "Full-duplex fiber-wireless link with 40 Gbit/s 16-QAM signals for alternative wired and wireless accesses based on homodyne/heterodyne coherent detection," *J. Opt. Fiber Technol.* **20**(3), 261–267 (2014).
13. J. Wang and J.-M. Kahn, "Impact of chromatic and polarization-mode dispersions on DPSK systems using interferometric demodulation and direct detection," *J. Lightwave Technol.* **22**(2), 362–371 (2004).
14. R. A. Shafik, S. Rahman, and R. Islam, "On the extended relationships among EVM, BER and SNR as performance metrics," in *Int. Conf. on Electrical and Computer Engineering*, pp. 408–411, IEEE (2006).
15. D. Hillerkuss et al., "26 Tbits-1 line-rate super-channel transmission utilizing all-optical fast Fourier transform processing," *Nat. Photonics* **5**(6), 364–371 (2011).

Ruijiao Zhang is a doctoral student at Beijing University of Posts and Telecommunications, Beijing, China. Her current research focuses on radio-over-fiber technologies, hybrid wired/wireless access technologies, and W-band wireless access technologies.

Jianxin Ma is an associate professor at Beijing University of Posts and Telecommunications. He received his PhD degree in optical communication from Beijing University of Posts and Telecommunications, Beijing, China, in 2007. He has authored or coauthored more than 50 scientific publications appearing in journals or international conferences. His main research interests include the applications of microwave photonics to telecommunications systems and radio-over-fiber technologies.

Xiangjun Xin: Biography is not available.